

Article

A Study on Assimilation of CYGNSS Wind Speed Data for Tropical Convection during 2018 January MJO

Xuanli Li ^{1,*} , John R. Mecikalski ¹ and Timothy J. Lang ² ¹ University of Alabama in Huntsville, Huntsville, AL 35805, USA; johnm@nsstc.uah.edu² NASA Marshall Space Flight Center, Huntsville, AL 35812, USA; timothy.j.lang@nasa.gov

* Correspondence: xuanli@nsstc.uah.edu

Received: 27 February 2020; Accepted: 10 April 2020; Published: 14 April 2020



Abstract: The National Aeronautics and Space Administration (NASA) Cyclone Global Navigation Satellite System (CYGNSS) mission was launched in December 2016. CYGNSS provides ocean surface wind speed retrieval along specular reflection tracks at an interval resolution of approximately 25 km. With a median revisit time of 2.8 h covering a $\pm 35^\circ$ latitude, CYGNSS can provide more frequent and accurate measurements of surface wind over the tropical oceans under heavy precipitation, especially within tropical cyclone cores and deep convection regions, than traditional scatterometers. In this study, CYGNSS v2.1 Level 2 wind speed data were assimilated into the Weather Research and Forecasting (WRF) model using the WRF Data Assimilation (WRFDA) system with hybrid 3- and 4-dimensional variational ensemble technology. Case studies were conducted to examine the impact of the CYGNSS data on forecasts of tropical cyclone (TC) Irving and a westerly wind burst (WWB) during the Madden–Julian oscillation (MJO) event over the Indian Ocean in early January 2018. The results indicate a positive impact of the CYGNSS data on the wind field. However, the impact from the CYGNSS data decreases rapidly within 4 h after data assimilation. Also, the influence of CYGNSS data only on precipitation forecast is found to be limited. The assimilation of CYGNSS data was further explored with an additional experiment in which CYGNSS data was combined with Global Precipitation Mission (GPM) Integrated Multi-satellite Retrievals for GPM (IMERG) hourly precipitation and Advanced Scatterometer (ASCAT) wind vector and were assimilated into the WRF model. A significant positive impact was found on the tropical cyclone intensity and track forecasts. The short-term forecast of wind and precipitation fields were also improved for both TC Irving and the WWB event when the combined satellite data was assimilated.

Keywords: CYGNSS; data assimilation; tropical cyclone; tropical convection; MJO

1. Introduction

Owing to better global analyses and advances in numerical models and physics parameterizations, tropical cyclone (TC) forecasts have improved steadily in the past two decades (See, e.g., [1,2]). Despite the substantial amount of effort, however, accurate predictions of the structure and intensity of TCs and tropical convections remain challenging. The structure and intensity of TCs are not only influenced by the large-scale environment; the air–sea exchange also plays a vital role. The variations in structure and intensity also depend largely on the meso- and micro- scale in-storm dynamic, physics, and radiative processes, as well as the interaction of environmental flow and storm-scale processes [3,4]. An accurate description of the atmospheric state and the environment is essential for simulations of tropical cyclones and tropical convections.

Since tropical cyclones and maritime tropical convection spend most of their lifetime over oceans where conventional data and aircraft measurements are limited in space and time, the need for a more

accurate representation of storms and their environment motivates the application of satellite-retrieved products. Satellite wind products, especially the surface wind from scatterometers, can provide information about the location and intensity of tropical cyclones and tropical convections. However, these observation systems [e.g., Quick Scatterometer—QuikSCAT, Advanced Scatterometer—ASCAT, and OceanSat-2 Scatterometer—OSCAT] suffer from severe limitations under extreme conditions (e.g., heavy precipitation, strong winds $> 35 \text{ m s}^{-1}$, etc.), and long revisit times ($\sim 12+$ h) also limit their usefulness in detecting rapid changes in intensity and location [5,6]. To obtain ocean surface wind data with high-spatial and temporal resolutions, and in adverse surface weather conditions of thick clouds and precipitation, the Cyclone Global Navigation Satellite System (CYGNSS) mission was launched in December 2016 [7]. The CYGNSS constellation is composed of eight bistatic microsatellites in a slightly elliptical orbit plane, at a 35° inclination angle, and between roughly 510 and 540 km altitude. As low Earth orbiting (LEO) satellites, CYGNSS provides a relatively frequent revisit time, with a median value of 2.8 h and a mean of 7.2 h [7,8]. Each CYGNSS microsatellite is equipped with a Delay Doppler Mapping Instrument (DDMI) that consists of a multichannel Global Navigation Satellite System reflectometry (GNSS-R) receiver, a low-gain zenith antenna to receive the direct global positioning system (GPS) signals, and two high-gain downward pointing antennas to receive the scattered GPS signals from the ocean surface [9,10]. CYGNSS measures the pattern and intensity of the scattered and reflected GPS signals at specular reflection points within the $\pm 35^\circ$ latitude coverage zone. CYGNSS uses the GPS “L1” channel, which suffers no appreciable attenuation, even under heavy rainfall conditions. This allows CYGNSS to retrieve ocean surface winds for a variety of tropical phenomena, e.g., the tropical cyclone core region and deep convection associated with the Madden–Julian Oscillation (MJO; [11,12]), with a level of accuracy that was previously impossible in practice. Each CYGNSS observatory is capable of sampling 4 different specular reflection tracks at a frequency of 1 Hz, and ocean surface wind speed is retrieved along the specular tracks at a resolution of approximately 25 km. It is expected that the CYGNSS will be able to accurately monitor the rapidly changing wind of precipitating regions over the tropics (e.g., [13]), and to improve forecasting operations (e.g., [14]).

Numerical models commonly struggle in predicting the accurate intensity of TCs. It is especially challenging to capture the rapid intensity change of TCs during the intensification or weakening stages [15]. Another great challenge in forecasts of TCs and tropical convections is the wind speed distribution, especially over large variability regions [16,17]. Many studies have shown that the assimilation of wind observations is an effective method to improve the initial condition of numerical weather prediction (NWP) models, and hence, to improve intensity and wind predictions of TCs and tropical convection. A number of studies (e.g., [18–23]) have shown that the assimilation of in situ wind data from dropwindsondes and flight level airborne surveillance provided significant improvements in TC track and intensity forecasts. The assimilation of satellite-derived motion vector winds has improved forecast skills of global and regional NWP models at operation centers, such as the National Centers for Environmental Prediction (NCEP), the European Centre for Medium-Range Weather Forecasts (ECMWF), the United Kingdom Met Office, and the Korea Meteorological Agency [24–27]. Ocean surface winds, including retrievals from QuikSCAT, ASCAT, and OSCAT, are especially useful for improving TC position, intensity, and structure by providing additional measurements of enhancements of the air-sea exchange and the cyclonic circulation [28–34]. Prior to the use of real CYGNSS data, a number of previous studies evaluated the assimilation of the CYGNSS data derived from an end-to-end simulator into observing system simulation experiments (OSSEs). Their results suggested that the simulated CYGNSS data would positively impact the forecasts of TCs in both track and intensity [35–39]. The assimilation of real CYGNSS observation was recently investigated by Cui et al. [14]; the authors indicated the potential of CYGNSS data in improving the track, intensity, and structure of TCs. Unfortunately, due to data quality issues, Cui et al. [14] were only able to assimilate CYGNSS v2.0 fully developed seas (FDS) data, which greatly underestimates the wind field within deep convection regions related to TCs. A recent study (Ruf et al. [40]) indicated that, with a

number of improvements to the data calibration, v2.1 is of much better quality than the previous version; this is especially true for the young seas/limited fetch (YSLF) product. Ruf et al. [41] calculated the root-mean-square (RMS) difference between CYGNSS v2.0 YSLF data and Stepped Frequency Microwave Radiometers (SFMRs) data onboard the NOAA P-3 aircraft in and near hurricanes. For wind retrievals above 20 m s^{-1} , the RMS was 5.01 m s^{-1} when the uncertainty of the SFMR measurements was removed. When CYGNSS v2.1 YSLF data were evaluated, Ruf et al. [40] indicated that this RMS value had been reduced to 3.2 m s^{-1} . In the current study, we examined the assimilation of both FDS and YSLF v2.1 wind speed products. Through the present study, our objectives are: (1) to evaluate the impact and reveal the challenge of utilizing the CYGNSS ocean surface wind speed data in a numerical model, and (2) to explore how to better utilize the CYGNSS data and improve short-term forecast skill.

2. Data and Methods

2.1. Data

The main datasets used in this study include the Level 2 CYGNSS version 2.1 data, Global Precipitation Mission (GPM) Integrated Multi-satellitE Retrievals for GPM (IMERG) data, and Level 2 ASCAT data. The CYGNSS Level 2 data is obtainable from the Physical Oceanography Distributed Active Archive Center (PODAAC) (<https://podaac-tools.jpl.nasa.gov/drive/files/OceanWinds/cygnss/L2/v2.1>). The GPM IMERG is a Level 3 gridded product for global rainfall estimates. Its spatial resolution is 0.1° and temporal resolution is 0.5 h. The IMERG product incorporates precipitation estimates from GPM and partner satellite microwave and infrared (IR) sensors. Rain gauge data was used in calibration of IMERG [42]. GPM IMERG rainfall data is available at <https://pmm.nasa.gov/data-access/downloads/gpm>. ASCAT is one of several instruments on the Meteorological Operational (MetOp) polar-orbiting satellite. It is an active microwave sensor designed to provide surface wind observations over the global oceans. The ASCAT ocean surface wind vector data has a resolution of 25 km and is available twice a day over the model domain. ASCAT data can be accessed from the PODAAC (<https://podaac-tools.jpl.nasa.gov/drive/files/OceanWinds/ascat>).

2.2. The 2018 January MJO and CYGNSS Observation

The MJO is the dominant mode of intraseasonal variability (30–90 days), characterized by eastward propagation of enhanced deep convection at an average speed of 5 m s^{-1} during boreal winter [43]. The MJO convective signal typically initiates in the Indian Ocean and propagates to (and often across) the Maritime Continent to the western Pacific. The Real-time Multivariate MJO (RMM) index [44] is a commonly used index in MJO studies and operation forecasts as a measure of the phase and intensity of an MJO event. Figure 1 illustrates the RMM index provided by the Australian Bureau of Meteorology (data available at <http://www.bom.gov.au/climate/mjo/graphics/rmm.74toRealtime.txt>) from late December 2017 to early February 2018. RMM1 and RMM2 represent the first and second principal components of the combined empirical orthogonal functions (EOFs) of outgoing longwave radiation (OLR), as well as zonal wind at 200 and 850 hPa averaged between 15°N and 15°S . Points outside the center circle indicate a significant MJO event; the farther from the origin, the stronger the MJO amplitude. The phase triangles indicate the primary location of Indian Ocean, Maritime Continent, western Pacific, or western hemisphere and Africa. The 2018 MJO was one of the strongest events in the last few decades [45]. Barrett [45] showed that the MJO progressed eastward in January from the Indian Ocean to the Pacific Ocean in February, and then back to the Indian Ocean in March. The apparent counterclockwise motion shown in Figure 1a indicates the eastward propagation of the event. As in Figure 1a, the MJO was in phases 2 and 3 over the Indian Ocean from January 1 to 16, with maximum RMM of 2.1. The MJO intensified as it passed through Maritime Continent (Phases 4 and 5) from January 17 to 26. The MJO was strong in the western Pacific in phases 6 and 7 from January 27 to February 4, with a peak RMM close to 4. Hoover et al. [46] found that synthetic CYGNSS observations were able to measure outflow from convective storms in simulated MJO events

from October and December 2011. Figure 1b shows the CYGNSS surface wind speed averaged over the domain 70° – 80° E and 0° – 10° S from 1 to 31 January 2018. This is within the core initiation region of the MJO in the Indian Ocean. The average CYGNSS wind speed showed a peak of 8 m s^{-1} on 7–8 January, which is in agreement with the maximum RMM value at the same time in phases 2 and 3. A trough in the average CYGNSS wind speed with a magnitude lower than 4 m s^{-1} occurred in 12–16 January. This is also in agreement with the low RMM index in 10–15 January shown in Figure 1a. Another period of large CYGNSS wind over 7 m s^{-1} occurred during 24–29 January 2018, which also coincides with strong convection and increasing RMM values during that time period as the MJO signal transitioned to the Maritime Continent. This indicates that, in general, CYGNSS data were able to detect strong winds related to this MJO event. However, it is noteworthy that the average CYGNSS wind speed calculated here is sensitive to WWBs during the MJO, and also to any weather system enhancing wind speeds within the domain; thus this metric should not be viewed as a definitive measure of MJO strength. The late January enhancement in CYGNSS wind speed appears to be similar to that of early January, with an enhanced near-Equator westerly flow associated with the presence of TC Cebile.

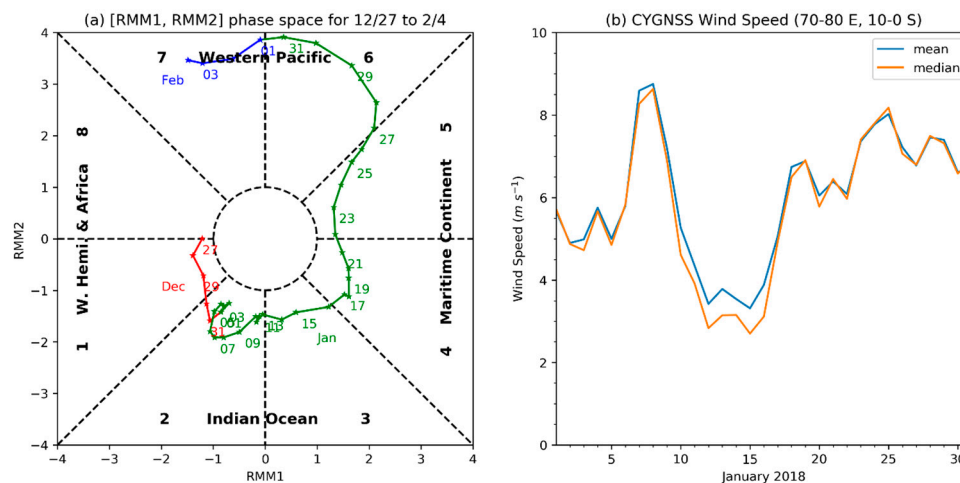


Figure 1. (a) RMM index phase diagram from 27 December 2017 to 4 February 2018. Different color lines represent the different months (red for December, green for January, and blue for February); dates are annotated to the left of the values. Phases are labelled on the diagram. Points outside the circle indicate a significant MJO event, while phase triangles indicate its primary location. (b) CYGNSS daily wind speed averaged within 70° – 80° E, 10° S– 0° .

Previous studies found that CYGNSS measurements during TC overpasses can help in finding the correct center location, estimating the intensity, and constructing the wind distribution within the TC [40,47,48]. Hoover et al. [46] also showed that synthetic CYGNSS data may be used to monitor westerly wind burst (WWB) events during MJO events. In this study, we will examine the CYGNSS data for TC Irving and a WWB event during the 2018 January MJO, and evaluate the impact of the CYGNSS data on the short-term numerical prediction of these events.

TC Irving initiated from a low-pressure system in the southern Indian Ocean at ~ 1800 UTC on 4 January 2018 and developed into a tropical storm after 18 h. It continued to strengthen and became a tropical cyclone by 0600 UTC on 7 January, with the center minimum sea level pressure (MSLP) falling to 981 hPa and the maximum surface winds reaching 36 m s^{-1} . TC Irving gained further intensity as it moved southwestward, and reached peak intensity with a MSLP of 962 hPa and maximum surface wind of 49 m s^{-1} at 0000 UTC on 8 January. Thereafter, it started to weaken before it dissipated at around 0600 UTC on 11 January 2018. In this study, we focused on the intensification from 0000 UTC on 6–8 January, and the weakening afterwards until 0000 UTC on 9 January 2018.

In this study, a few quality control steps were applied to the Level 2 CYGNSS data v2.1. Data with the range corrected gain below 3 and the zenith sun angle lower than zero were removed to filter out the

unreliable observations. Also, the uncertainties in the Block II-F GPS transmitter power and antenna gain patterns can significantly degrade the quality of wind speed products [49]. Therefore, all Level 2 retrievals from Block II-F GPS satellites were excluded from the Level 2 product. Further quality control (e.g., gross check, vertical consistency, dry convective adjustment, etc.) was conducted during WRFDA data process before the CYGNSS wind speed observation was assimilated. Two different wind speed products retrieved by different geophysical model functions (GMFs) are provided in v2.1, i.e., the FDS and the YSLF. The FDS is appropriate for most conditions, while the YSLF data can be used typically for the inner core of TCs. YSLF GMF was developed for conditions when the long-wave portion of the sea state has not responded fully to the local surface winds [40,41]. Figure 2 displays the sample data of the CYGNSS v2.1 YSLF (Figure 2a) product around 1500 UTC, and FDS product over-plotted on GPM IMERG rainfall (Figure 2b) at around 1500 UTC, and the ASCAT wind speed (Figure 2c) at 1448 UTC on 7 January 2018. In Figure 2, CYGNSS detected TC Irving with a maximum wind of 24 m s^{-1} in the FDS product and 44 m s^{-1} in the YSLF product over the heavily-precipitating eyewall region. ASCAT views could not penetrate the core region of TC Irving, but a maximum wind speed of 26 m s^{-1} was observed in the surrounding area. For the WWB event, IMERG data indicates that convection was observed with a maximum precipitation rate of around 10 mm h^{-1} . ASCAT observed a portion of the WWB event with maximum wind speed of 14 m s^{-1} . Strong winds related to this WWB event were detected by CYGNSS with a maximum wind speed of 17 m s^{-1} in the FDS product.

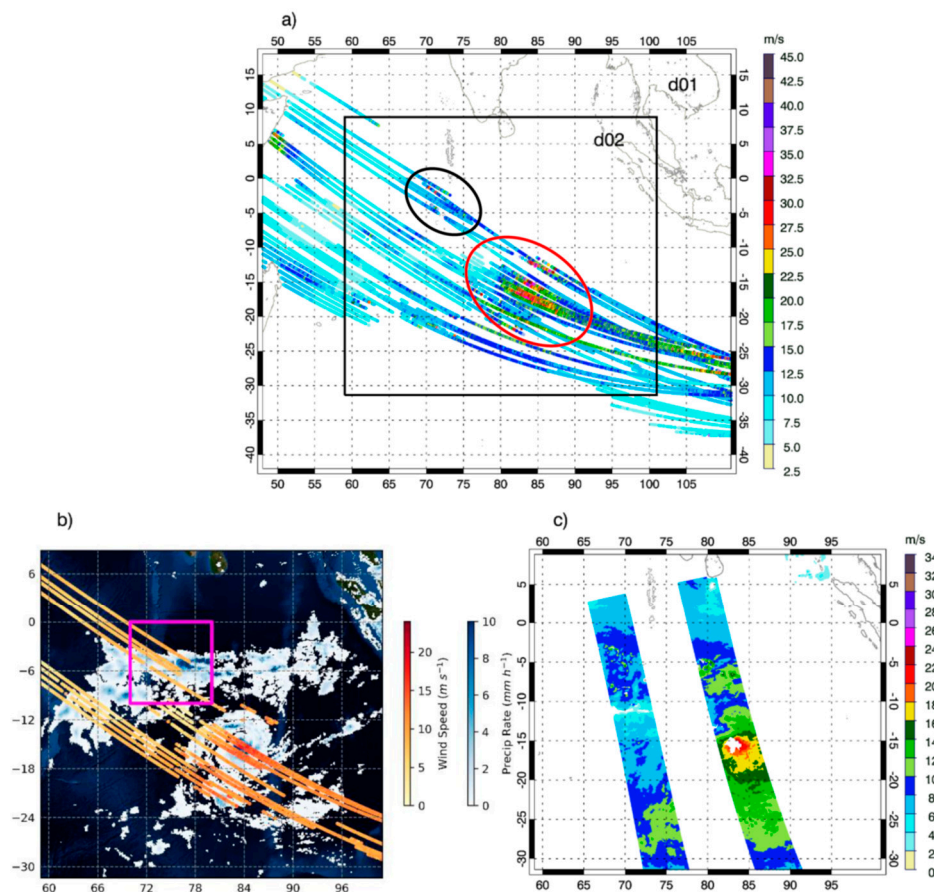


Figure 2. (a) WRF model 9-km and 3-km domains (d01 and d02) and CYGNSS v2.1 YSLF data within 1.5 h from 1500 UTC on 7 January 2018. The black circle shows the high winds in CYGNSS related to the WWB and the red circle shows high winds related to TC Irving. (b) CYGNSS v2.1 FDS data in 1400–1500 UTC over-plotted on IMERG 1-h rainfall at 1400 UTC on 7 January 2018. The magenta box shows the approximate location of the WWB event. (c) ASCAT wind speed at around 1448 UTC on 7 January 2018.

2.3. Data Assimilation Experiments

The advanced research Weather Research and Forecasting (WRF-ARW; [50]) model and the WRF Data Assimilation (WRFDA) system ([51]) were used in this study. The WRF model and WRFDA system are open-source and can be downloaded from <https://www2.mmm.ucar.edu/wrf/users/downloads.html>. This study used a double nested domain with resolutions of 9- and 3-km to simulate TC Irving and the WWB event (Figure 2a). The following model physics schemes were used: the rapid radiative transfer model (RRTM; [52]) long-wave radiation, Dudhia shortwave radiation [53], Betts-Miller-Janjic cumulus parameterization [54], Mellor-Yamada-Janjic (MYJ) planetary boundary layer (PBL) schemes [54], Morrison 2-moment microphysical scheme [55], and the Unified Noah land-surface model [56]. The cumulus parameterization was only used for the outer domain.

The WRFDA system was used to conduct data assimilation with the hybrid ensemble variational technique. WRFDA is a unified community data assimilation system that has 3-dimensional variational (3DVAR) and 4-dimensional ensemble variational (4DVAR) capabilities, a hybrid variational ensemble algorithm (EnVar) and ensemble transform Kalman Filter technique. Being built in model-space, WRFDA is a flexible, state-of-the-art atmospheric data assimilation system that is portable and efficient for various platforms and for multiple models. WRFDA is suitable for the assimilation of a wide variety of observations, including conventional surface and upper-air soundings, ship, buoy, aircraft, satellite retrieved products, satellite radiance, radar, surface precipitation, etc. In this research, data assimilation is conducted with “cv option 5” which defines streamfunction, unbalanced velocity potential, unbalanced temperature, pseudo relative humidity, and unbalanced surface pressure as the control variables. The wind observations were assimilated using the wind speed and direction assimilation package based on Huang et al. [57].

Four different experiments were conducted. Table 1 lists the observation data assimilated in each experiment and the data assimilation analysis times. All experiments began at 0000 UTC on 6 January and ended at 0000 UTC on 9 January 2018. The control experiment (CTRL) was a WRF regional simulation. The initial and boundary conditions were interpolated from the 0.25° resolution global NCEP Final Analysis (FNL). The impact of the CYGNSS data was firstly examined with two experiments—DA_cyg_fd and DA_cyg_lf, in which the 3-dimensional ensemble variational (3DEnVar) technique was adopted in the assimilation of only CYGNSS FDS and YSLF data, respectively. Ensemble WRF forecasts with 12 members were generated with randomly perturbed initial conditions created using the ensemble transform Kalman filter (ETKF) technique [58]. The ensemble forecast was used to produce a flow-dependent background error matrix. Cycled assimilation of the CYGNSS data was conducted at 0000, 1200, 1500, and 2100 UTC from 6 to 8 January, based on the data availability. There are more CYGNSS data available for TC Irving and the WWB event at 0000 and 1500 UTC than at other times. The observational error was set as 2 m s⁻¹ for winds below 20 m s⁻¹ and 10% for winds above 20 m s⁻¹ based on the general guidance from Ruf et al. [40]. If there were multiple observations within a model grid box, a distance-weighted average of all observations was calculated and assimilated. The last experiment (DA_com) assimilated the combined CYGNSS wind speed, IMERG rainrate, and ASCAT vector wind data using the 4-dimensional ensemble variational (4DEnVar) technique. The 4DEnVar also used 12-member ensemble WRF forecasts to generate the flow dependent background error matrix. In this experiment, the CYGNSS data include YSLF data within 800 km from the center of TC Irving and FDS data elsewhere. Figure 3 illustrates the time windows of the 4DEnVar process in DA_com.

Table 1. Numerical Experiments setup.

Experiment	Data	Data Assimilation Analysis Times
CTRL	N/A	N/A
DA_cyg_fd	CYGNSS FDS wind speed	0000, 1200, 1500, and 2100 UTC on 6–8 January 2018
DA_cyg_lf	CYGNSS YSLF wind speed	0000, 1200, 1500, and 2100 UTC on 6–8 January 2018
DA_com	Combined IMERG rainfall, ASCAT vector wind, and CYGNSS wind speed	0000, 0230, 1100, 1500, 2000, and 2300 UTC on 6 January; 0300, 1100, 1530, 2000, and 2300 UTC on 7 January; 0300, 1100, 1500, and 2000 UTC on 8 January 2018

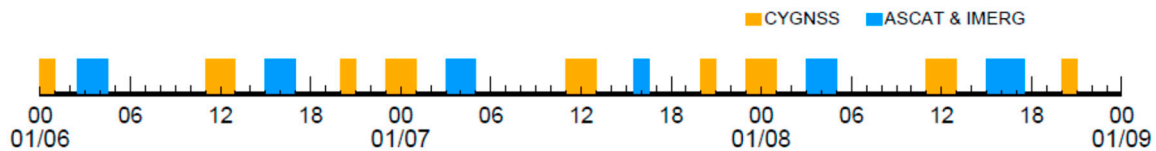


Figure 3. Data assimilation process for the experiment DA_com. Orange boxes show the time windows for CYGNSS data assimilation, and the blue boxes show the time windows when the ASCAT and IMERG data were assimilated. In the time window near 1500 UTC of each day, all three types of data were assimilated.

3. Results

3.1. CYGNSS Data Assimilation

To examine the impact of the CYGNSS wind speed data, the analysis fields and short-term forecasts from experiments with and without the assimilation of CYGNSS data are compared and analyzed in this section. Figure 4 plots the CYGNSS wind, background wind field, and data assimilation analysis increment (‘analysis – background’, or the difference between data assimilation analysis and the background) in the surface wind field at 1500 UTC on 6 January 2018. At this time, CYGNSS FDS (Figure 4a) observed a maximum wind speed of 18 m s^{-1} , with most of the observed wind being slower than 15 m s^{-1} , while CYGNSS YSLF (Figure 4b) detected wind as strong as 47 m s^{-1} near TC Irving and many points with wind speed above 15 m s^{-1} . In the background field (Figure 4e), an area of wind above 15 m s^{-1} was predicted over the eyewall region of TC Irving with the maximum wind speed of 20 m s^{-1} . Therefore, the wind speed observed by CYGNSS FDS is generally lower than the background. When the FDS data were assimilated, the analysis increments were mostly negative near TC Irving (Figure 4c). With the assimilation of high winds from CYGNSS YSLF data, the surface wind increased by up to 6 m s^{-1} near TC Irving and 2 m s^{-1} for the WWB event (Figure 4d). However, the limitation of assimilating the CYGNSS data was also apparent. Due to the track-based nature of CYGNSS observation, the analysis increment in DA_cyg_lf shows elongated shapes at several places. This very likely does not represent the correct characteristics of the wind field, and therefore, may cause inaccurate asymmetry in wind and, hence, mass fields.

The RMS difference in surface wind speed is calculated between the data assimilation experiments (DA_cyg_lf and DA_cyg_fd) and the background field, and averaged over the model domain. Figure 5 shows the domain averaged RMS difference of surface wind speed within 9 h after the assimilation of CYGNSS data was complete at 1500 UTC on 6 January 2018. At the analysis time, the averaged RMS was 1.2 m s^{-1} for DA_cyg_lf and 0.86 m s^{-1} for DA_cyg_fd. It rapidly declined for both experiments within the first hour after data assimilation. After 4 h, the averaged RMS were only 0.41 m s^{-1} and 0.32 m s^{-1} for DA_cyg_lf and DA_cyg_fd, which were 30% and 37% of the original values, respectively. This indicates that the strongest impact of the CYGNSS data will be within the first ~4 h of the forecast.

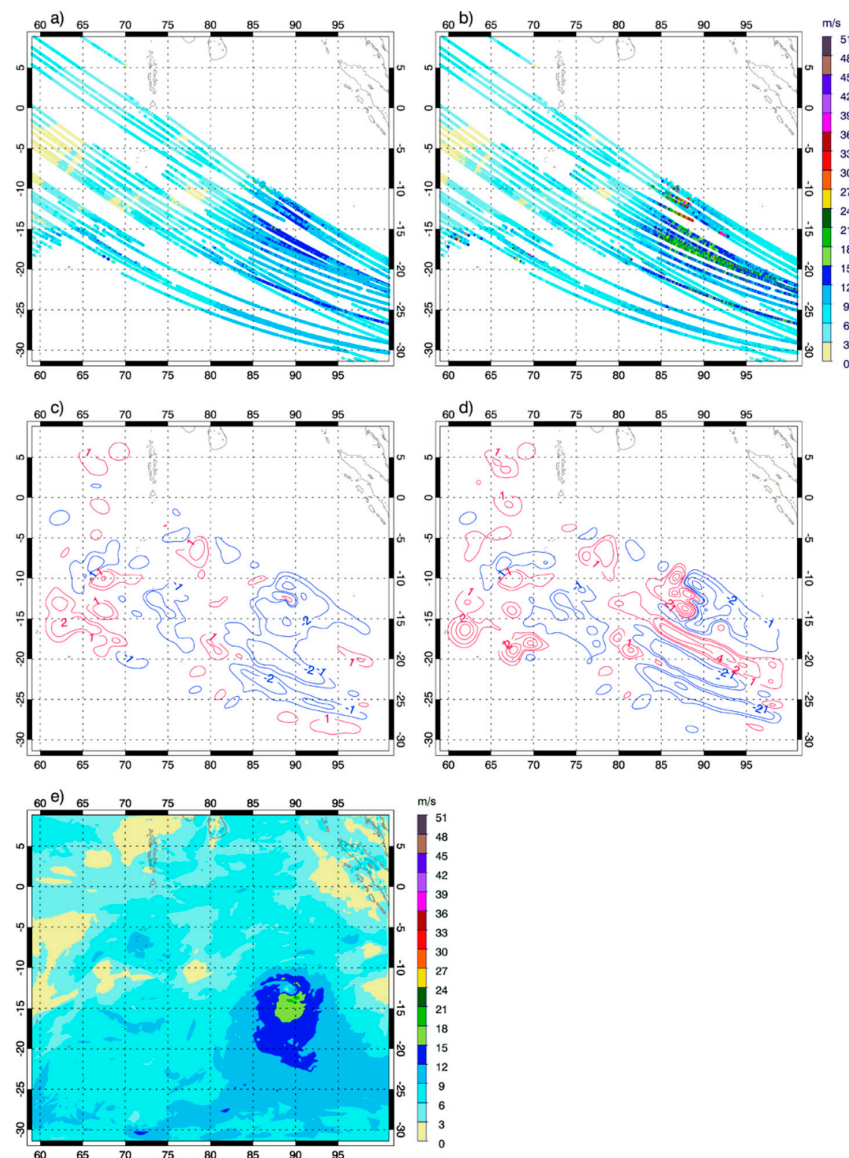


Figure 4. CYGNSS wind speed observation (a) FDS and (b) YSLF. The analysis increments from (c) DA_cyg_fd and (d) DA_cyg_lf. The blue contours represent negative values and red contours represent positive values. The contour interval is 1 m s^{-1} . (e) wind field in background WRF simulation. All plots are at 1500 UTC on 6 January 2018.

With the assimilation of CYGNSS data in the initial conditions, positive impacts have been made in the simulations of TC Irving and the WWB event. Figure 6 displays the surface wind field from DA_cyg_fd, DA_cyg_lf, and CTRL compared with ASCAT observation around 0239 UTC on 8 January 2018. ASCAT (Figure 6a) observed an area of wind speed over 18 m s^{-1} around the vortex with a maximum surface wind speed over 30 m s^{-1} . There is no apparent quadrant asymmetry in ASCAT data. In comparison, a strong quadrant asymmetry was found in all numerical experiments with the strongest wind appearing in the front-left quadrant. In addition, all three numerical experiments produced a larger area of wind speed $> 18 \text{ m s}^{-1}$. The best track data shows the maximum surface wind of 49 m s^{-1} (0000 UTC) to 46 m s^{-1} (0600 UTC) at this time. Therefore, all numerical experiments produced an underestimate of the storm intensity. With assimilation of the YSLF data, DA_cyg_lf (Figure 6d) generated a stronger TC than CTRL (Figure 6b) and DA_cyg_fd (Figure 4c). A smaller eye with stronger maximum surface wind speed (28 m s^{-1}) was found in DA_cyg_lf when comparing with CTRL (25 m s^{-1}) and DA_cyg_fd (22 m s^{-1}). Also note that the center location in the three experiments

are quite different. At this time, the observed storm center derived from the Joint Typhoon Warning Center (JTWC) best track data was near 79.9°E, 17.05°S. The 51-h forecast in CTRL predicted the storm center at 81.15°E, 18.5°S, which is 208-km away from the observed one. After seven cycles of CYGNSS data assimilation, the predicted center location was at 80.5°E, 18.5°S and 80.5°E, 17.8°S in DA_cyg_lf and DA_cyg_fd, respectively. Both forecasts were better than CTRL, with track errors of 174-km and 105-km for DA_cyg_lf and DA_cyg_fd, respectively.

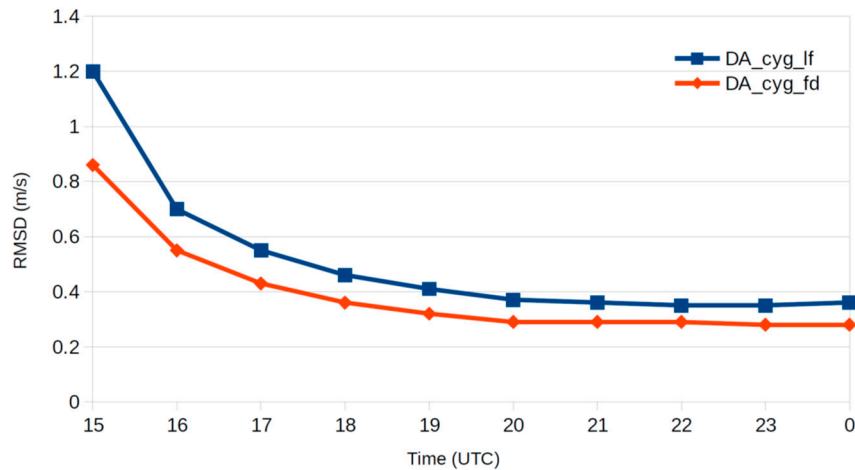


Figure 5. Time series of domain averaged RMS difference of surface wind speed between data assimilation experiments and the background field from 1500 UTC on 6 January 2018 to 0000 UTC on 7 January 2018.

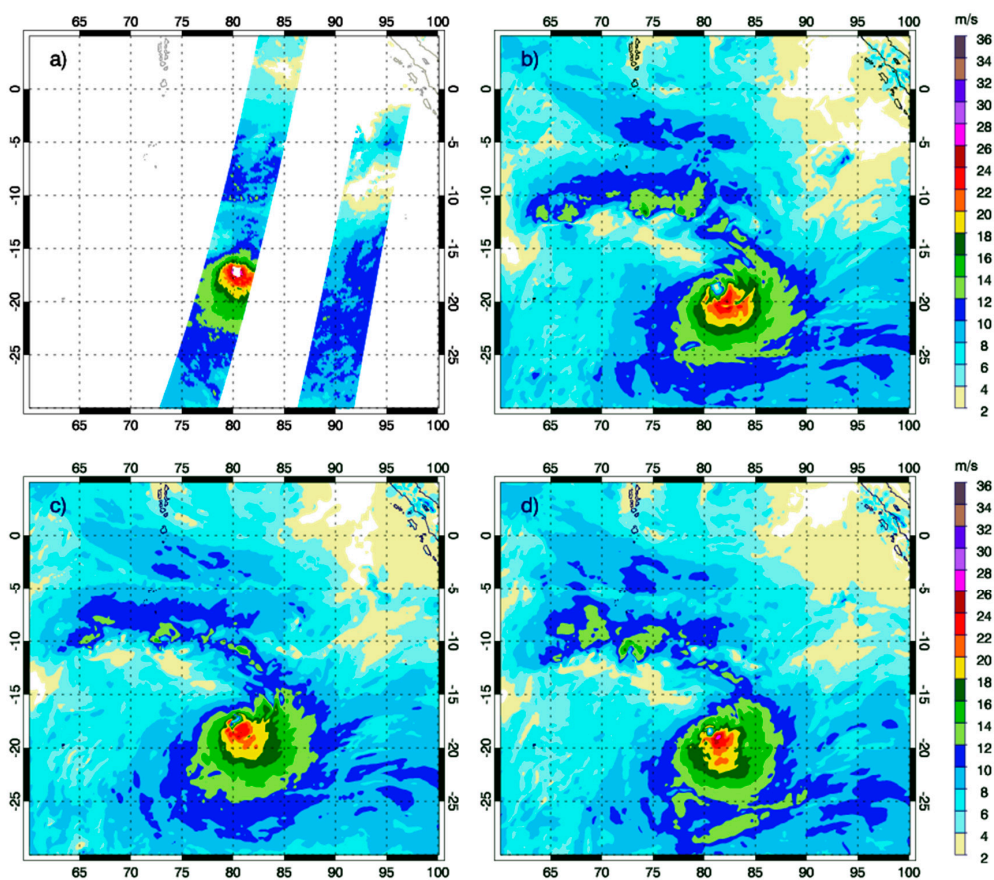


Figure 6. Surface wind speed from (a) ASCAT around 0239 UTC and (b) CTRL, (c) DA_cyg_fd, and (d) DA_cyg_lf at 0300 UTC on 8 January 2018.

The impact of CYGNSS data assimilation on the intensity and track forecasts of TC Irving was compared with the JTWC best track data in Figures 7 and 8. From 00 UTC on 6 January to 00 UTC on 8 January, TC Irving experienced an intensification, from a tropical storm to a category-2 tropical cyclone, with a peak intensity of 962 hPa in MSLP of and 49 m s^{-1} in maximum surface wind speed, followed by a weakening stage until 0000 UTC on 9 January with 973 hPa in MSLP of and 41 m s^{-1} in maximum surface wind speed. From Figure 7, CTRL greatly underestimated the intensity of TC Irving. The forecast in CTRL shows a slow strengthening of Irving from 999 hPa in MSLP and 17 m s^{-1} in maximum surface wind speed at 0000 UTC on 6 to 990 hPa and 25 m s^{-1} at 0000 UTC on 9 January 2018. Improvement in intensity forecast by the assimilation of the CYGNSS data was found from 0000 UTC on 7 January to 0000 UTC on 8 January 2018. During this time period, both DA_cyg_lf and DA_cyg_fd outperformed CTRL with the strongest storm generated by DA_cyg_lf. CTRL missed the weakening of the storm from 0000 UTC on 8 to 0000 UTC on 9 January 2018. The intensity of the storms in DA_cyg_lf and DA_cyg_fd showed some fluctuations, but no apparent weakening was predicted in either experiment. It is noteworthy that the intensity forecast in data assimilation experiments was not always better than CTRL (e.g., from 1200 UTC on 8 January to 0000 UTC on 9 January 2018 in DA_cyg_fd).

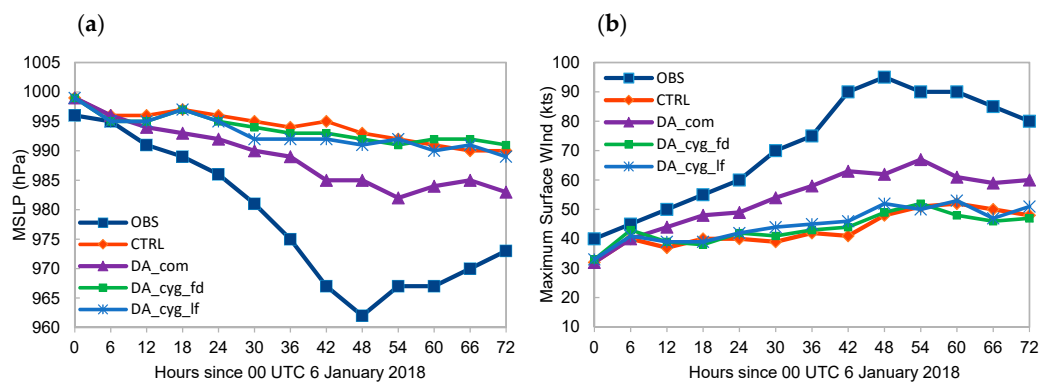


Figure 7. Time series of TC Irving intensity for (a) MSLP and (b) maximum surface wind speed from JTWC best track data, CTRL, DA_cyg_fd, DA_cyg_lf, and DA_com at 0000 UTC on 6–9 January 2018.

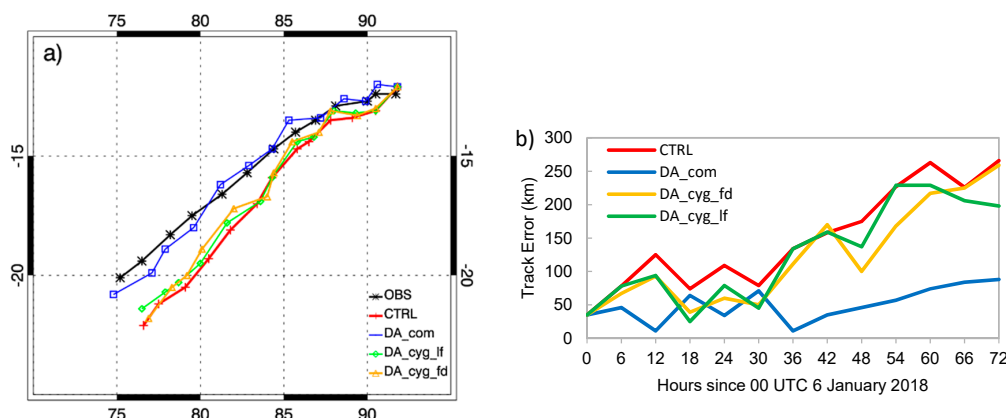


Figure 8. (a) TC Irving track from JTWC best track data, CTRL, DA_cyg_fd, DA_cyg_lf, and DA_com and (b) track error from CTRL, DA_cyg_fd, DA_cyg_lf, and DA_com at 0000 UTC on 6–9 January 2018.

The track forecasts from CTRL and data assimilation experiments were compared with the JTWC best track in Figure 8. As shown in Figure 8a, all experiments captured the southwestward path of TC Irving. CTRL produced the track to the south of the observed storm with a track error ranging from 35 km to 265 km. The assimilation of CYGNSS FDS data provided help with the tracking forecast. The track error in DA_cyg_fd was generally smaller than those of either CTRL or DA_cyg_lf, except at 1800 UTC on 7 January and in the last 6 h of the forecast period. For example, at 0000 UTC on 8 January,

the center location of TC Irving in DA_cyg_fd (the track error of 100 km) was much closer to the observed location when compared with the one in CTRL (the track error of 175 km) and the one in DA_cyg_lf (the track error of 137 km).

Figure 9 displays IMERG precipitation, CYGNSS FDS and YSLF wind speed, ASCAT wind speed and model simulated wind from DA_cyg_lf and CTRL over the region of the WWB event when ASCAT captured a portion of the event near 1500 UTC on 8 January 2018. IMERG (Figure 9a) shows the convection related to the WWB event produced a maximum precipitation over 10 mm h^{-1} . ASCAT (Figure 9b) indicates a large area with wind speed over 12 m s^{-1} and a maximum of 20 m s^{-1} . CYGNSS FDS (Figure 9c) detected weaker winds for the WWB with $< 10 \text{ m s}^{-1}$ at most points, and a maximum value of 12 m s^{-1} , while in YSLF data (Figure 9d), many points in the three tracks across the observed WWB region had wind speed $> 12 \text{ m s}^{-1}$ with a maximum of 27 m s^{-1} . The assimilation of high winds in YSLF data explains the apparent increase in the analysis wind field. Surface wind speed in DA_cyg_lf (Figure 9f) exceeded 14 m s^{-1} over the storm area, while the surface wind speed in CTRL (Figure 9e) was generally below 12 m s^{-1} .

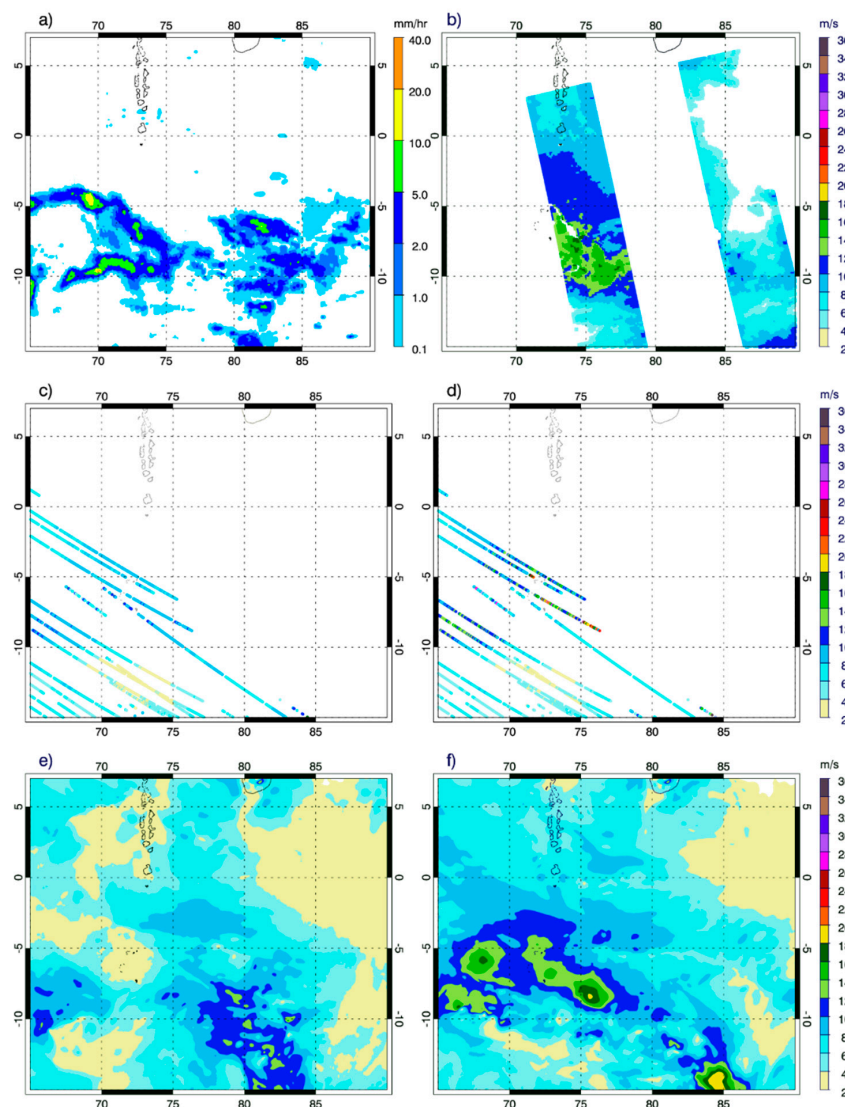


Figure 9. (a) IMERG precipitation for the WWB event at 1500 UTC on 8 January 2018, (b) ASCAT wind speed around 1436 UTC on 8 January 2018, (c) CYGNSS FDS and (d) YSLF wind speed around 1500 UTC on 8 January 2018, and surface wind speed from (e) CTRL and (f) DA_cyg_lf at 1500 UTC on 8 January 2018.

The overall impacts of the CYGNSS observation on surface wind and precipitation fields are shown in Tables 2 and 3. Table 2 lists the domain averaged RMS of surface wind speed difference between different experiments and ASCAT wind speed within the model domain available around 0302 and 1448 UTC on 7 January and 0239 and 1436 UTC on 8 January 2018. As shown in the table, the assimilation of both CYGNSS FDS and YSLF data led to smaller RMS values at all times. At 1500 UTC on 8 January, the RMS reduced by up to 0.7 m s^{-1} in DA_cyg_lf when comparing with CTRL. Table 3 lists the threat scores (TS) of precipitation forecast with a threshold value of 2 mm h^{-1} from different experiments. The IMERG data were used as the reference dataset. The TS was calculated using the equation from Xiao et al. [59]:

$$TS = \frac{C}{F + R + C} \quad (1)$$

where C is the number of correct forecast events (points with precipitation exceeding the threshold value), R is the number of events in observation, and F is the number of events in forecast. As indicated in Table 3, the differences in TSs between CTRL and the data assimilation experiments DA_cyg_fd and DA_cyg_lf were as small as 0.01–0.02, which indicates that the influence from assimilation of CYGNSS data only was not significant. This could be attributed to the continuous correction of model dynamics, which commonly occurs when only surface data are assimilated. Another possible reason is the lack of dynamic support from the convective and thermodynamic fields for convection to grow. This was the motivation for the DA_com data assimilation experiment, as described next.

Table 2. Domain averaged RMS difference of surface wind speed between ASCAT observation and different numerical experiments.

Experiment	0300 UTC on 7 January 2018	1500 UTC on 7 January 2018	0300 UTC on 8 January 2018	1500 UTC on 8 January 2018
CTRL	2.63	2.92	3.12	3.67
DA_cyg_fd	2.55	2.43	2.85	3.08
DA_cyg_lf	2.45	2.37	2.70	2.97
DA_com	1.54	1.47	1.70	2.08

Table 3. Threat Score of precipitation forecast with threshold value of 2 mm h^{-1} 0000 UTC on 8–9 January 2018 for different experiments with IMERG rainfall as the reference dataset.

Experiment	0000 UTC on 8 January 2018	0600 UTC on 8 January 2018	1200 UTC on 8 January 2018	1800 UTC on 8 January 2018	0000 UTC on 9 January 2018
CTRL	0.18	0.19	0.17	0.14	0.15
DA_cyg_fd	0.19	0.18	0.17	0.15	0.16
DA_cyg_lf	0.19	0.19	0.18	0.16	0.15
DA_com	0.38	0.35	0.34	0.32	0.33

3.2. Assimilation of the Combined Satellite Datasets

The above results indicate the positive impacts of CYGNSS data, as well as the limitations of the CYGNSS data when being assimilated into the initial conditions of NWP simulations. Since the IMERG data can measure the precipitation of tropical convection, the ASCAT data can describe the cyclonic circulation of TCs, and the CYGNSS data can provide wind speed observations under heavy precipitation, it would be of great interest to examine how the combined datasets would help with TC and tropical convection intensity and structure.

The overall performance of DA_com is compared with other experiments in Tables 2 and 3. As shown in Table 2, DA_com produced the lowest RMS values at all times among all experiments. Specifically, the domain averaged RMS values in DA_com ranged from 1.47 to 2.08 m s^{-1} . When comparing to CTRL, the RMS values reduced by 1.09 to 1.59 m s^{-1} , indicating a 41–49%

relative reduction. From Table 3, it is shown that the precipitation forecast skill in DA_com was apparently higher than the rest of the experiments. For example, the TS in CTRL was only 0.15 at 0000 UTC on 9 January 2018, while the value in DA_com was 0.33, which is a relative improvement of 120%. These results indicate large positive impacts with the assimilation of the combined datasets.

To illustrate the prediction of intensity and structure of TC Irving, Figure 10 shows a comparison of the sea level pressure (SLP) over-plotted on surface wind from DA_com and CTRL near TC Irving from around 0300 UTC on 7 January and 1500 UTC on 8 January 2018, when ASCAT observation was available. At both times, DA_com produced better intensity estimates than CTRL compared to the best track data. At 0300 UTC on 7 January, the best track data showed that TC Irving had a MSLP between 986 hPa (0000 UTC) and 981 hPa (0600 UTC) and a maximum surface wind speed between 31 m s^{-1} (0000 UTC) and 36 m s^{-1} (0600 UTC). ASCAT (Figure 10a) missed the strong wind in the core region due to contamination by heavy precipitation. Therefore, the wind asymmetry of TC Irving is unclear. CTRL (Figure 10b) produced a weak storm with a MSLP of 995 hPa and maximum wind of 20 m s^{-1} , while DA_com (Figure 10c) was able to generate a stronger cyclone with a MSLP of 992 hPa and maximum wind of 30 m s^{-1} . The strongest wind appeared at the front left quadrant of TC Irving in DA_com and at the front in CTRL, respectively. At 1500 UTC on 8 January, the best track data shows that the intensity of the storm was between 967 hPa (1200 UTC) and 970 hPa (1800 UTC) in MSLP, and 47 m s^{-1} (1200 UTC) to 44 m s^{-1} (1800 UTC) in maximum surface wind speed. ASCAT (Figure 10d) observed the maximum wind speed of 28 m s^{-1} with a small eye. CTRL (Figure 10e) underestimated TC Irving with a MSLP of 991 hPa and a maximum wind speed of 27 m s^{-1} . A better intensity and wind field was produced in DA_com (Figure 10f) with a MSLP of 982 hPa and a maximum surface wind speed of 32 m s^{-1} and a smaller eye. From ASCAT, it seems that the strongest wind at this time appeared at the front right quadrant of TC Irving, and that there was no apparent wind asymmetry around the eyewall. In CTRL, the strongest wind was at the front to front left of TC Irving with a strong wind asymmetry. DA_com shows the strong wind occurring in both front left and front right quadrants. The asymmetry was not as apparent as the wind field in CTRL.

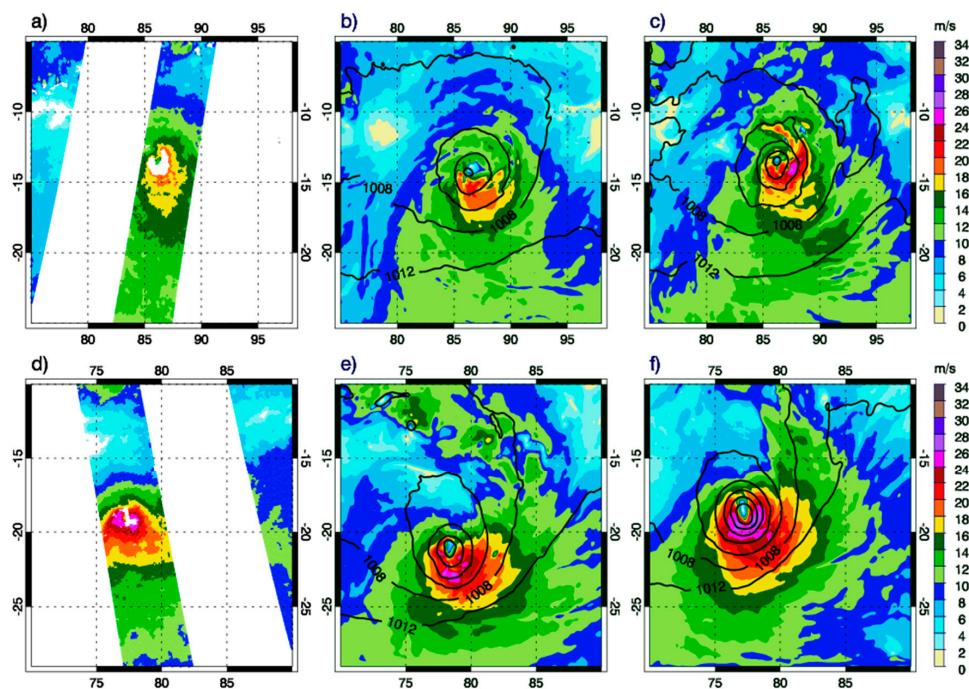


Figure 10. Surface wind speed near TC Irving from (a) ASCAT observation at 0302 UTC, and surface wind speed prediction overplotted with sea level pressure from (b) CTRL, and (c) DA_com at 0300 UTC on 7 January 2018; and (d) ASCAT at 1436 UTC, and surface wind speed with sea level pressure from (e) CTRL, and (f) DA_com at 1500 UTC on 8 January 2018.

Figure 11 shows the surface wind field for the WWB event around 1500 UTC on 7 January and 1600 UTC on 8 January 2018 when ASCAT captured a portion of the event. At both times, DA_com produced stronger wind field than CTRL. ASCAT (Figure 11a,d) shows wind speed $> 8 \text{ m s}^{-1}$ over the area $65^{\circ}\text{--}85^{\circ}\text{E}$ and $10^{\circ}\text{S--}0^{\circ}$ with a maximum wind speed of 16 m s^{-1} . CTRL (Figure 11b,e) predicted much smaller areas that have wind speed $> 8 \text{ m s}^{-1}$ with the maximum of 13 m s^{-1} . In comparison, DA_com (Figure 11c,f) produced large areas with wind speed over 8 m s^{-1} and a maximum wind of 18 m s^{-1} . The location of the WWB was also better predicted in DA_com at 1600 UTC on 8 January 2018.

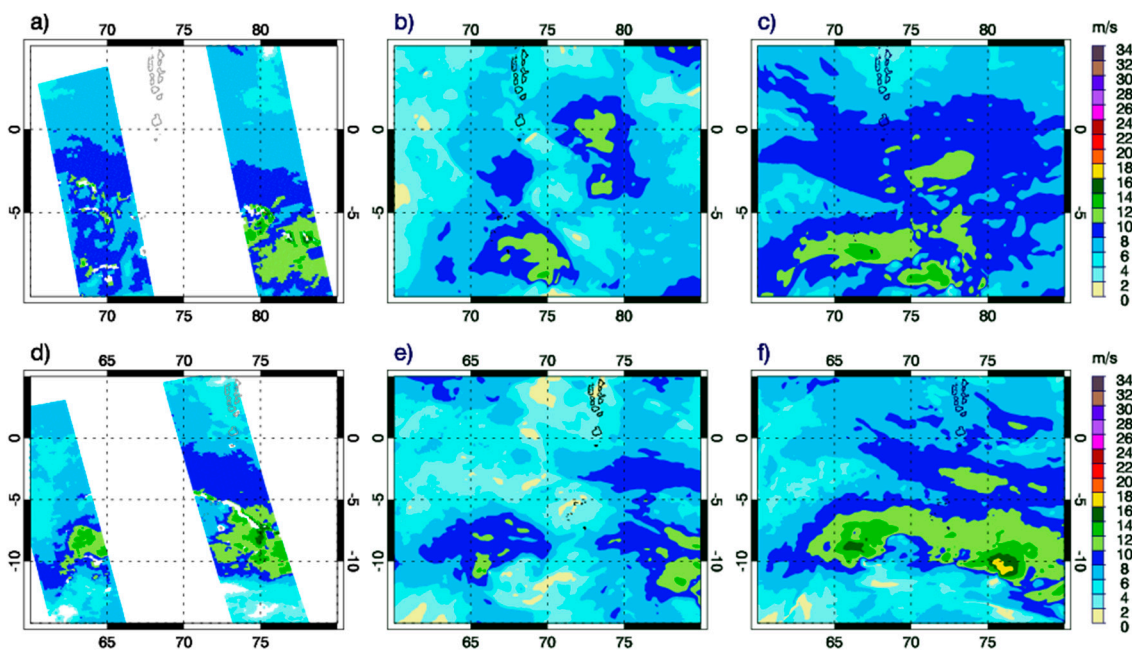


Figure 11. Surface wind speed near the WWB event from (a) ASCAT observation around 1448 UTC, and prediction from (b) CTRL, and (c) DA_com at 1500 UTC on 7 January 2018; and (d) ASCAT around 1524 UTC, and surface wind prediction from (e) CTRL, and (f) DA_com at 1600 UTC on 8 January 2018.

Figure 12 compares the precipitation predictions from CTRL and DA_com with IMERG data at 1500 UTC on 7 January and 2100 UTC on 8 January 2018. At both times, DA_com generated a much stronger and better organized precipitation over the core region of TC Irving than CTRL. At 1500 UTC on 7 January, DA_com (Figure 12c) produced maximum rainfall of 36 mm h^{-1} around the eyewall, which was pretty close to the observed 34 mm h^{-1} by IMERG (Figure 12a), and 12 mm h^{-1} higher than the one predicted in CTRL (Figure 12b). At 2100 UTC on 8 January 2018, both DA_com and CTRL underestimated the precipitation for TC Irving. IMERG (Figure 12d) estimated the maximum rainfall rate of 56 mm h^{-1} . CTRL (Figure 12e) predicted maximum rainfall of 20 mm h^{-1} . DA_com (Figure 12f) outperformed CTRL with a much stronger precipitation field with a maximum of 42 mm h^{-1} . Precipitation related to the WWB event was also better represented in DA_com (Figure 13). At 1200 UTC on 7 January 2018, IMERG observed strong convection with the maximum precipitation rate of 32 mm h^{-1} at $75^{\circ}\text{--}80^{\circ}\text{E}$ and $5^{\circ}\text{--}7^{\circ}\text{S}$. In CTRL, this storm was not predicted. With the assimilation of the combined datasets, DA_com produced heavy precipitation near the observed location with the maximum precipitation $> 40 \text{ mm h}^{-1}$. A similar result was found at 2100 UTC on 8 January 2018. IMERG observed convection with maximum precipitation of 23 mm h^{-1} at $67^{\circ}\text{--}78^{\circ}\text{E}$ and $4^{\circ}\text{--}8^{\circ}\text{S}$. CTRL predicted multiple strong convective storms, but the locations were far from the observed one. DA_com was able to generate the precipitation at $70^{\circ}\text{--}78^{\circ}\text{E}$ and $4^{\circ}\text{--}8^{\circ}\text{S}$ with maximum precipitation of 26 mm h^{-1} .

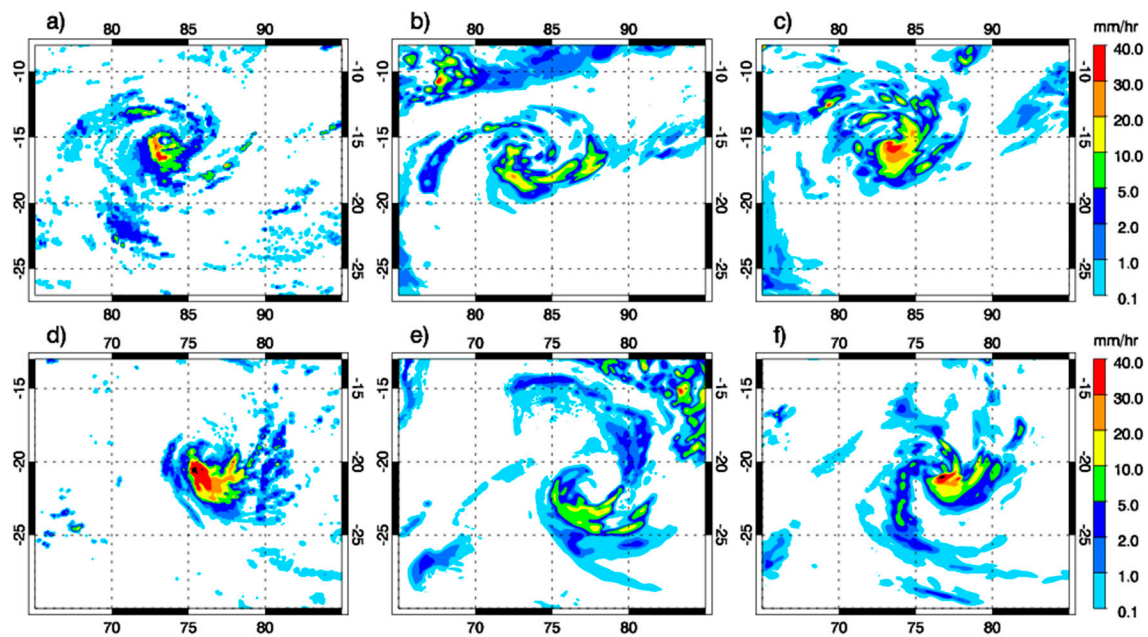


Figure 12. 1-h precipitation around TC Irving from (a) IMERG, (b) CTRL, (c) DA_com at 1500 UTC on 7 January 2018 and (d) IMERG, (e) CTRL, and (f) DA_com at 2100 UTC on 8 January 2018.

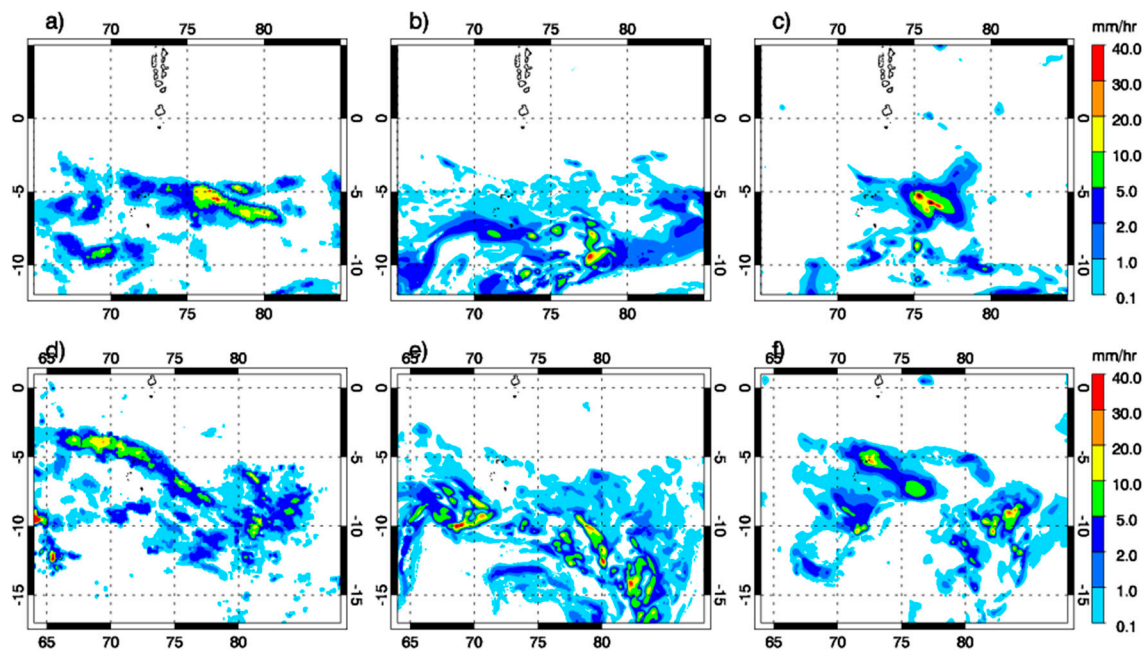


Figure 13. 1-h precipitation for convection related to the WWB event from (a) IMERG, (b) CTRL, (c) DA_com at 1200 UTC on 7 January 2018 and (d) IMERG, (e) CTRL, and (f) DA_com at 2100 UTC on 8 January 2018.

The impacts of the combined satellite datasets on the intensity and track of TC Irving are displayed in Figures 7 and 8. As shown in Figure 7, DA_com also underestimated the intensity of TC Irving, but apparently performed better when comparing to CTRL, DA_cyg_fd, and DA_cyg_lf. An intensification was predicted from 999 hPa in MSLP and 17 m s^{-1} in maximum surface wind speed at 0000 UTC on 6 January to 985 hPa and 35 m s^{-1} at 1800 UTC on 7 January 2018. The weakening after 0600 UTC on 8 January was also captured. With the assimilation of the combined satellite datasets, the track forecast of TC Irving in DA_com was also improved. The center locations in DA_com were very close to the observed ones with the track error ranges from 11 km at 1200 UTC on 6 January 2018

to 88 km at 0000 UTC on 9 January 2018. In comparison, the track errors were 125, 93, and 94 km at 1200 UTC on 6 January 2018, and 266, 259, 198 km at 0000 UTC on 9 January 2018 in CTRL, DA_cyg_fd, and DA_cyg_lf, respectively.

4. Discussion

In this study, the application of CYGNSS v2.1 Level 2 data was examined in a numerical simulation of TC Irving and a WWB event that occurred during the 2018 January MJO event. WRF model simulations and WRFDA 3DEnVar and 4DEnVar data assimilation experiments were conducted to investigate the impact of the CYGNSS data when it was assimilated individually, as well as combined with the IMERG rainfall and ASCAT ocean surface wind vector observations. The goal of this study was to report on the benefits and challenge in the assimilation of CYGNSS data.

The results indicate that CYGNSS data can capture the high winds and sharp wind gradient under heavily precipitating conditions within TC Irving and the WWB event. When CYGNSS data were assimilated individually, a positive impact was found on the wind field for both TC Irving and the WWB event. The intensity and track forecast of TC Irving were also positively affected. However, the main impact of the data appears to only last about 4 h. In addition, the influence of the CYGNSS winds on the precipitation field was modest at best. When CYGNSS winds were assimilated together with IMERG hourly rainfall and ASCAT ocean surface vector winds, significant impacts were found in the wind, pressure, and precipitation fields. The intensity and track forecast of TC Irving were largely improved. Specifically, the structure in wind and precipitation fields in the vicinity of the TC core region and across the WWB event was better represented with the assimilation of the combined satellite data. Unfortunately, one caveat of the current research is the lack of an experiment parallel to DA_com that assimilates IMERG and ASCAT data using 4DEnVar. Due to the expensive computational cost of 4DEnVar, we did not have the time or computational resource to conduct this experiment. Therefore, the sole impact of CYGNSS data is unclear when IMERG and ASCAT data are also assimilated. This is quite important for a thorough understanding on the overall benefit and limitation of CYGNSS observation. In future studies, we will conduct these experiments with more case studies to further explore the impact of CYGNSS data when it is combined with other datasets.

5. Conclusions

The results shown here are quite encouraging. However, the conclusions in this study are based on only one case study. More experiments with additional cases for a variety of tropical weather systems are needed to demonstrate a thorough evaluation of the consistent impacts of the CYGNSS observations to NWP forecasts. New versions of the CYGNSS data (v3.0 and Climate Data Record—CDR v1.0) are expected to be available soon; v3.0 includes a near-real-time corrections for variations in the transmit power of the GPS satellites, and is expected to improve the temporal and spatial sampling properties, as well as the accuracy. CDR data include track-wise debiasing that is expected to improve wind speed calibration. In both new data versions, a reduction is expected in the uncertainty of the wind speed products for both high and low wind speed [40]. Therefore, future research should be conducted with WRF simulations and data assimilation experiments for new versions of CYGNSS data to further explore the application of the latest products. In addition, the frequent revisit time of CYGNSS is one of the great advantages of this instrument. Hence, it would be of great interest to conduct continuous assimilation of CYGNSS data and to investigate the benefit it may bring to midrange to subseasonal forecasts of tropical convection and MJO events.

Author Contributions: Conceptualization, X.L., J.R.M., and T.J.L.; Methodology, X.L., J.R.M., and T.J.L.; Software, X.L. and T.J.L.; Validation, X.L., J.R.M., and T.J.L.; Formal analysis, X.L., J.R.M., and T.J.L.; Investigation, X.L., J.R.M., and T.J.L.; Resources, X.L., J.R.M., and T.J.L.; Data curation, X.L. and T.J.L.; Writing—original draft preparation, X.L., J.R.M., and T.J.L.; Writing—review and editing, X.L., J.R.M., and T.J.L.; Visualization, X.L., J.R.M., and T.J.L.; Supervision, J.R.M. and T.J.L.; Project administration, J.R.M. and T.J.L.; Funding acquisition, X.L., J.R.M., and T.J.L. All authors have read and agreed to the published version of the manuscript.

Funding: This research was funded by NASA, grant number NNM11AA01A.

Acknowledgments: The authors also acknowledge the NASA CYGNSS science and operations team for providing the observational data. The authors would like to thank the anonymous reviewers for their valuable comments and suggestions to make the paper having a much improved quality.

Conflicts of Interest: The authors declare no conflict of interest.

References

1. Cangialosi, J.; Franklin, J. 2016 Hurricane Season. National Hurricane Center Forecast Verification Report. 2017; p. 72. Available online: https://www.nhc.noaa.gov/verification/pdfs/Verification_2016.pdf (accessed on 12 April 2020).
2. Yamaguchi, M.; Ishida, J.; Sato, H.; Nakagawa, M. WGNE intercomparison of tropical cyclone forecasts by operational NWP models: A quarter century and beyond. *Bull. Am. Meteorol. Soc.* **2017**, *98*, 2337–2349. [[CrossRef](#)]
3. Minamide, M.; Zhang, F. Adaptive observation error inflation for assimilating all-sky satellite radiance. *Mon. Weather Rev.* **2017**, *145*, 1063–1081. [[CrossRef](#)]
4. Ito, K. Errors in tropical cyclone intensity forecast by RSMC Tokyo and statistical correction using environmental parameters. *SOLA* **2016**, *12*, 247–252. [[CrossRef](#)]
5. Quilfen, Y.; Chapron, B.; Tournadre, J. Satellite microwave surface observations in tropical cyclones. *Mon. Weather Rev.* **2010**, *138*, 421–437. [[CrossRef](#)]
6. Liu, W.; Tang, W. Relating wind and stress under tropical cyclones with scatterometer. *J. Atmos. Ocean. Technol.* **2016**, *33*, 1151–1158. [[CrossRef](#)]
7. Ruf, C.S.; Atlas, R.; Chang, P.; Clarizia, M.; Garrison, J.; Gleason, S.; Katzberg, S.; Jelenak, Z.; Johnson, J.; Majumdar, S.; et al. New Ocean Winds Satellite Mission to Probe Hurricanes and Tropical Convection. *Bull. Am. Meteorol. Soc.* **2016**, *97*, 385–395. [[CrossRef](#)]
8. Ruf, C.; Chang, P.; Clarizia, M.; Gleason, S.; Jelenak, Z.; Murray, J.; Morris, M.; Musko, S.; Posselt, D.; Provost, D.; et al. *CYGNSS Handbook*; The University of Michigan: Ann Arbor, MI, USA, 2016; p. 154. ISBN 978-1-60785-380-0.
9. Rose, R.; Dickinson, J.; Ridley, A. CubeSats to NanoSats; Bridging the gap between educational tools and science workhorses. In Proceedings of the 2012 IEEE Aerospace Conference, Big Sky, MT, USA, 3–10 March 2012. [[CrossRef](#)]
10. Ruf, C.; Gleason, S.; Jelenak, Z.; Katzberg, S.; Ridley, A.; Rose, R.; Scherrer, J.; Zavorotny, V. The CYGNSS nanosatellite constellation hurricane mission. In Proceedings of the 2012 IEEE International Geoscience and Remote Sensing Symposium, Munich, Germany, 22–27 July 2012; p. 214. [[CrossRef](#)]
11. Madden, R.; Julian, P. Detection of a 40–50 day oscillation in the zonal wind in the tropical Pacific. *J. Atmos. Sci.* **1971**, *28*, 702–708. [[CrossRef](#)]
12. Madden, R.; Julian, P. Description of global-scale circulation cells in the Tropics with a 40–50 day period. *J. Atmos. Sci.* **1972**, *29*, 1109–1123. [[CrossRef](#)]
13. Park, J.; Johnson, J.; Yi, Y.; O'Brien, A. Using “Rapid Revisit” CYGNSS Wind Speed Measurements to Detect Convective Activity. *IEEE J. Sel. Top. Appl. Earth Obs. Remote Sens.* **2018**, *12*, 98–106. [[CrossRef](#)]
14. Cui, Z.; Pu, Z.; Tallapragada, V.; Atlas, R.; Ruf, C. A preliminary impact study of CYGNSS ocean surface wind speeds on numerical simulations of hurricanes. *Geophys. Res. Lett.* **2019**, *46*, 2984–2992. [[CrossRef](#)]
15. Brown, D. Tropical Cyclone Intensity Forecasting: Still a Challenging Proposition. National Hurricane Center; 2017. Available online: https://www.nhc.noaa.gov/outreach/presentations/NHC2017_IntensityChallenges.pdf (accessed on 12 April 2020).
16. Tyner, B.; Aiyyer, A.; Blaes, J.; Hawkins, D. An examination of wind decay, sustained wind speed forecasts, and gust factors for recent tropical cyclones in the mid-Atlantic region of the United States. *Weather Forecast.* **2015**, *30*, 153–176. [[CrossRef](#)]
17. Goldenberg, S.; Gopalakrishnan, S.; Tallapragada, V.; Quirio, T.; Marks, F.; Trahan, S.; Zhang, X.; Atlas, R. The 2012 triply nested, high-resolution operational version of the Hurricane Weather Research and Forecasting Model (HWRF): Track and intensity forecast verifications. *Weather Forecast.* **2015**, *30*, 710–728. [[CrossRef](#)]

18. Aberson, S.D.; Franklin, J.L. Impact on hurricane track and intensity forecasts of GPS dropwindsonde observations from the first-season flights of the NOAA Gulfstream-IV jet aircraft. *Bull. Am. Meteorol. Soc.* **1999**, *80*, 421–427. [[CrossRef](#)]
19. Aberson, S.D. The impact of dropwindsonde data from the THORPEX Pacific Area Regional Campaign and the NOAA hurricane field program on tropical cyclone forecasts in the Global Forecast System. *Mon. Weather Rev.* **2011**, *139*, 2689–2703. [[CrossRef](#)]
20. Chou, K.-H.; Wu, C.-C.; Lin, P.-H.; Aberson, S.D.; Weissmann, M.; Harnisch, F.; Nakazawa, T. The impact of dropwindsonde observations on typhoon track forecasts in DOTSTAR and T-PARC. *Mon. Weather Rev.* **2011**, *139*, 1728–1743. [[CrossRef](#)]
21. Wu, C.C.; Lin, P.H.; Aberson, S.; Yeh, T.C.; Huang, W.P.; Chou, K.H.; Hong, J.S.; Lu, G.C.; Fong, C.T.; Hsu, K.C.; et al. Dropwindsonde Observations for Typhoon Surveillance near the Taiwan Region (DOTSTAR): An overview. *Bull. Am. Meteorol. Soc.* **2005**, *86*, 787–790. [[CrossRef](#)]
22. Weng, Y.; Zhang, F. Advances in convection-permitting tropical cyclone analysis and prediction through EnKF assimilation of reconnaissance aircraft observations. *J. Meteorol. Soc. Jpn.* **2016**, *94*, 345–358. [[CrossRef](#)]
23. Christophersen, H.; Aksoy, A.; Dunion, J.; Aberson, S. Composite impact of Global Hawk unmanned aircraft dropwindsondes on tropical cyclone analyses and forecasts. *Mon. Weather Rev.* **2018**, *146*, 2297–2314. [[CrossRef](#)]
24. Bormann, N.; Salonen, K.; Peubey, C.; McNally, T.; Lupu, C. An overview of the status of the operational assimilation of AMVs at ECMWF. In Proceedings of the 11th International Winds Workshop, Auckland, New Zealand, 20–24 February 2012; EUMETSAT: Auckland, New Zealand, 2012. Available online: https://www.eumetsat.int/website/home/News/ConferencesandEvents/DAT_2039311.html (accessed on 12 April 2020).
25. Cotton, J.; Forsythe, M. AMVs at the Met Office: Activities to improve their impact in NWP. In Proceedings of the 11th International Winds Workshop, Auckland, New Zealand, 20–24 February 2012; EUMETSAT: Auckland, New Zealand, 2012. Available online: https://www.eumetsat.int/website/home/News/ConferencesandEvents/DAT_2039311.html (accessed on 12 April 2020).
26. Lee, E.; Kim, Y.; Sohn, E.; Cotton, J.; Saunders, R. Application of hourly COMS AMVs in KMA operation. In Proceedings of the 11th International Winds Workshop, Auckland, New Zealand, 20–24 February 2012; EUMETSAT: Auckland, New Zealand, 2012. Available online: https://www.eumetsat.int/website/home/News/ConferencesandEvents/DAT_2039311.html (accessed on 12 April 2020).
27. Su, X.; Daniels, J.; Derber, J.; Lin, Y.; Bailey, A.; Bresky, W.; Qi, H. Assimilation of GOES hourly AMVs in NCEP global data assimilation and forecast system. In Proceedings of the 12th International Winds Workshop, Copenhagen, Denmark, 16–20 June 2014; EUMETSAT: Copenhagen, Denmark, 2014. Available online: https://www.eumetsat.int/website/home/News/ConferencesandEvents/DAT_2441511.html?lang=EN (accessed on 12 April 2020).
28. Chen, S.-H. The impact of assimilating SSM/I and QuikSCAT satellite winds on Hurricane Isidore simulation. *Mon. Weather Rev.* **2007**, *135*, 549–566. [[CrossRef](#)]
29. Singh, R.; Pal, P.; Kishtawal, C.; Joshi, P. The impact of variational assimilation of SSM/I and QuikSCAT satellite observations on the numerical simulation of Indian Ocean tropical cyclones. *Weather Forecast.* **2008**, *23*, 460–476. [[CrossRef](#)]
30. Pu, Z.; Li, X.; Velden, C.; Aberson, S.; Liu, W. Impact of aircraft dropsonde and satellite wind data on the numerical simulation of two landfalling tropical storms during TCSP. *Weather Forecast.* **2008**, *23*, 62–79. [[CrossRef](#)]
31. Prasad, V.; Gupta, A.; Rajagopal, E.; Basu, S. Impact of OScat surface wind data on T574L64 assimilation and forecasting system—A study involving tropical cyclone Thane. *Curr. Sci.* **2013**, *104*, 627–631.
32. Liu, F.; Krieger, J.; Zhang, J. Toward producing the Chukchi–Beaufort High-Resolution Atmospheric Reanalysis (CBHAR) via the WRFDA data assimilation system. *Mon. Weather Rev.* **2014**, *142*, 788–805. [[CrossRef](#)]
33. Holt, C.; Szunyogh, I.; Gyarmati, G.; Leidner, S.; Hoffman, R. Assimilation of tropical cyclone observations: Improving the assimilation of TC Vitals, scatterometer winds, and dropwindsonde observations. *Mon. Weather Rev.* **2015**, *143*, 3956–3980. [[CrossRef](#)]
34. Laloyaux, P.; Thépaut, J.; Dee, D. Impact of scatterometer surface wind data in the ECMWF coupled assimilation system. *Mon. Weather Rev.* **2016**, *144*, 1203–1217. [[CrossRef](#)]

35. McNoldy, B.; Annane, B.; Majumdar, S.J.; Delgado, J.; Bucci, L.; Atlas, R. Impact of CYGNSS data on hurricane analyses and forecasts in a regional OSSE framework. *Mar. Technol. Soc. J.* **2017**, *51*, 7–15. [[CrossRef](#)]
36. Zhang, S.; Pu, Z.; Posselt, D.; Atlas, R. Impact of CYGNSS ocean surface wind speeds on numerical simulations of a hurricane in observing system simulation experiments. *J. Atmos. Ocean. Technol.* **2017**, *34*, 375–383. [[CrossRef](#)]
37. Annane, B.; McNoldy, B.; Leidner, S.M.; Hoffman, R.; Atlas, R.; Majumdar, S.J. A study of the HWRF analysis and forecast impact of realistically simulated CYGNSS observations assimilated as scalar wind speeds and as VAM wind vectors. *Mon. Weather Rev.* **2018**, *146*, 2221–2236. [[CrossRef](#)]
38. Leidner, S.M.; Annane, B.; McNoldy, B.; Hoffman, R.; Atlas, R. Variational analysis of simulated ocean surface winds from the Cyclone Global Navigation Satellite System (CYGNSS) and evaluation using a regional OSSE. *J. Atmos. Ocean. Technol.* **2018**, *35*, 1571–1584. [[CrossRef](#)]
39. Ying, Y.; Zhang, F. Potentials in Improving Predictability of Multiscale Tropical Weather Systems Evaluated through Ensemble Assimilation of Simulated Satellite-Based Observations. *J. Atmos. Sci.* **2018**, *75*, 1675–1698. [[CrossRef](#)]
40. Ruf, C.S.; Asharaf, S.; Balasubramaniam, R.; Gleason, S.; Lang, T.; McKague, D.; Twigg, D.; Waliser, D. In-orbit performance of the constellation of CYGNSS hurricane satellites. *Bull. Am. Meteorol. Soc.* **2019**, *100*, 2009–2023. [[CrossRef](#)]
41. Ruf, C.S.; Gleason, S.; McKague, D.S. Assessment of CYGNSS wind speed retrieval uncertainty. *IEEE J. Sel. Top. Appl. Earth Obs. Remote Sens.* **2018**, 1–11. [[CrossRef](#)]
42. Huffman, G.J.; Bolvin, D.T.; Nelkin, E.J. *Integrated Multi-satellitE Retrievals for GPM (IMERG) Technical Documentation*; NASA/GSFC Code 612 Tech. Doc.; IMERG Tech Document: Greenbelt, MD, USA, 2015; p. 48. Available online: http://pmm.nasa.gov/sites/default/files/document_files/IMERG_doc.pdf (accessed on 12 April 2020).
43. Zhang, C. Madden-Julian oscillation. *Rev. Geophys.* **2005**, *43*. [[CrossRef](#)]
44. Wheeler, M.C.; Hendon, H.H. An all-season real-time multivariate MJO index: Development of an index for monitoring and prediction. *Mon. Weather Rev.* **2004**, *132*, 1917–1932. [[CrossRef](#)]
45. Barrett, B.S. Connections between the Madden–Julian oscillation and surface temperatures in winter 2018 over eastern North America. *Atmos. Sci. Lett.* **2019**, *20*, e869. [[CrossRef](#)]
46. Hoover, K.E.; Mecikalski, J.; Lang, T.; Li, X.; Castillo, T.; Chronis, T. Use of an End-to-End-Simulator to analyze CYGNSS. *J. Atmos. Oceanic. Technol.* **2018**. [[CrossRef](#)]
47. Morris, M.; Ruf, C.S. Determining tropical cyclone surface wind speed structure and intensity with the CYGNSS satellite constellation. *J. Appl. Meteorol. Climatol.* **2017**, *56*, 1847–1865. [[CrossRef](#)]
48. Mayers, D.; Ruf, C. Tropical cyclone center fix using CYGNSS winds. *J. Appl. Meteorol. Climatol.* **2019**, *58*, 1993–2003. [[CrossRef](#)]
49. Ruf, C.; Balasubramaniam, R. Development of the CYGNSS geophysical model function for wind speed. *IEEE J. Sel. Top. Appl. Earth Obs. Remote Sens.* **2018**, *12*, 66–77. [[CrossRef](#)]
50. Skamarock, W.C.; Klemp, J.B.; Dudhia, J.; Gill, D.O.; Barker, D.; Duda, M.G.; Huang, X.Y.; Wang, W.; Powers, J.G. *A Description of the Advanced Research WRF Version 3*; NCAR Tech. Note, NCAR/TN-4751STR.; University Corporation for Atmospheric Research: Boulder, CO, USA, 2008; p. 113. [[CrossRef](#)]
51. Barker, D.M.; Huang, W.; Guo, Y.; Xiao, Q. A three-dimensional (3DVAR) data assimilation system for use with MM5: Implementation and initial results. *Mon. Weather Rev.* **2004**, *132*, 897–914. [[CrossRef](#)]
52. Mlawer, E.J.; Taubman, S.J.; Brown, P.D.; Iacono, M.J.; Clough, S.A. Radiative transfer for inhomogeneous atmosphere: RRTM, a validated correlated-k model for the longwave. *J. Geophys. Res.* **1997**, *102*, 16663–16682. [[CrossRef](#)]
53. Dudhia, J. Numerical study of convection observed during the winter monsoon experiment using a mesoscale two-dimensional model. *J. Atmos. Sci.* **1989**, *46*, 3077–3107. [[CrossRef](#)]
54. Janjic, Z.I. The step-mountain eta coordinate model: Further developments of the convection, viscous sublayer and turbulence closure schemes. *Mon. Weather Rev.* **1994**, *122*, 927–945. [[CrossRef](#)]
55. Morrison, H.; Thompson, G.; Tatarskii, V. Impact of cloud microphysics on the development of trailing stratiform precipitation in a simulated squall line: Comparison of one- and two-moment schemes. *Mon. Weather Rev.* **2009**, *137*, 991–1007. [[CrossRef](#)]

56. Chen, F.; Dudhia, J. Coupling an advanced land-surface/ hydrology model with the Penn State/ NCAR MM5 modeling system. Part I: Model description and implementation. *Mon. Weather Rev.* **2001**, *129*, 569–585. [[CrossRef](#)]
57. Huang, X.-Y.; Gao, F.; Jacobs, N.; Wang, H. Assimilation of wind speed and direction observations: A new formulation and results from idealised experiments. *Tellus A* **2013**, *65*, 19936. [[CrossRef](#)]
58. Wang, X.; Barker, D.M.; Snyder, C.; Hamill, T.M. A hybrid ETKF–3DVAR data assimilation scheme for the WRF Model. Part I: Observing system simulation experiment. *Mon. Weather Rev.* **2008**, *136*, 5116–5131. [[CrossRef](#)]
59. Xiao, Q.; Kuo, Y.; Sun, J.; Lee, W.; Lim, E.; Guo, Y.; Barker, D. Assimilation of Doppler Radar Observations with a Regional 3DVAR System: Impact of Doppler Velocities on Forecasts of a Heavy Rainfall Case. *J. Appl. Meteorol.* **2005**, *44*, 768–788. [[CrossRef](#)]



© 2020 by the authors. Licensee MDPI, Basel, Switzerland. This article is an open access article distributed under the terms and conditions of the Creative Commons Attribution (CC BY) license (<http://creativecommons.org/licenses/by/4.0/>).